



HAL
open science

Molecular dynamics simulation of the interaction of an Ar/CH₄ plasma with a surface: Growth, structure, and sputtering of the deposited C:H films

Glenn Otakandza Kandjani, Pascal Brault, Maxime Mikikian, Armelle Michau, Khaled Hassouni

► **To cite this version:**

Glenn Otakandza Kandjani, Pascal Brault, Maxime Mikikian, Armelle Michau, Khaled Hassouni. Molecular dynamics simulation of the interaction of an Ar/CH₄ plasma with a surface: Growth, structure, and sputtering of the deposited C:H films. *Plasma Processes and Polymers*, In press, 10.1002/ppap.202400084 . hal-04609808

HAL Id: hal-04609808

<https://hal.science/hal-04609808>

Submitted on 12 Jun 2024



HAL is a multi-disciplinary open access archive for the deposit and dissemination of scientific research documents, whether they are published or not. The documents may come from teaching and research institutions in France or abroad, or from public or private research centers.

L'archive ouverte pluridisciplinaire **HAL**, est destinée au dépôt et à la diffusion de documents scientifiques de niveau recherche, publiés ou non, émanant des établissements d'enseignement et de recherche français ou étrangers, des laboratoires publics ou privés.



Distributed under a Creative Commons Attribution 4.0 International License

Molecular dynamics simulation of the interaction of an Ar/CH₄ plasma with a surface: Growth, structure, and sputtering of the deposited C:H films

Glenn Otakandza Kandjani¹ | Pascal Brault¹  | Maxime Mikikian¹ |
Armelle Michau²  | Khaled Hassouni²

¹GREMI, UMR7344, CNRS/Université d'Orléans, Orleans, France

²LSPM, UPR3407, CNRS/Université Sorbonne Paris Nord, Villetaneuse, France

Correspondence

Pascal Brault, GREMI, CNRS, Université d'Orléans, 45067 Orléans Cedex 2, Orléans, France.

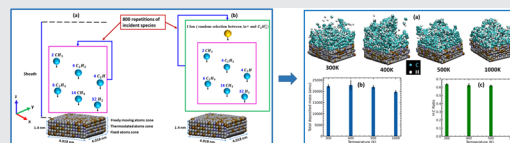
Email: pascal.brault@univ-orleans.fr

Funding information

National Scholarship Agency of Gabon (ANBG) and the French National Research Agency (ANR) through the MONA project, Grant/Award Number: ANR-18-CE30-0016; Fédération Calcul Scientifique et Modélisation Orléans Tours (CaSciModOT)

Abstract

Molecular dynamics simulations were performed to investigate the growth of hydrocarbon films with a surface at temperatures from 300 to 1000 K. The results show that C₂H is the main precursor of film growth. The formed C:H films are mainly unsaturated and dominated by double bonds and CN³ carbon atoms. The evolution of the C:H film is considered under the bombardment of the two major ions (Ar⁺ and C₂H₃⁺) with energies ranging from 50 to 100 eV. Film sputtering is significant above 50 eV, while at lower energies, the atoms of the C₂H₃⁺ ions can be incorporated and contribute to the growth.



KEYWORDS

film growth, hydrocarbon plasma, ion bombardment, molecular dynamics

1 | INTRODUCTION

Carbon-based thin films or hydrocarbon coatings are widely used for a variety of applications in different technological fields, from microelectronics, solar cells, and wearable electronics to optics/photonics, biotechnology, aerospace, energy, textiles, and many others.^[1–3]

Among the techniques used to ensure better and improved properties and functionalities of high-quality thin films, plasma- and vapor-phase-based techniques appear to be the most suitable and widely used approaches.^[1] The use of plasmas for thin-film

deposition is often grouped under the term plasma-enhanced chemical vapor deposition.^[1,4] Synthesized films are classified depending on their properties, with widespread names being diamond-like carbon and amorphous hydrogenated carbon (a-C:H). Depending on plasma parameters, the film properties can be varied from soft (polymer-like) to extremely hard (diamond-like), and a smooth transition between these two carbon families prevents a clear distinction.^[5] The acronym C:H (which is also used in this paper) is, therefore, used to denote all types of hydrogenated carbon films, and a-C:H is used only to denote hard films in accordance with common

This is an open access article under the terms of the [Creative Commons Attribution](https://creativecommons.org/licenses/by/4.0/) License, which permits use, distribution and reproduction in any medium, provided the original work is properly cited.

© 2024 The Author(s). *Plasma Processes and Polymers* published by Wiley-VCH GmbH.

usage, although this convention is not logical since soft films are also amorphous.^[5]

The fragmentation of the initial monomer molecules by electron impact is the first step in the process of film growth and leads to the formation of a wide variety of neutrals, radicals, and positive and negative ions. C:H films can be formed directly by exposing the sample surfaces to the plasma or indirectly by moving the sample away from the plasma volume, leaving the surface exposed only to diffusing reactive species.^[6,7] C:H films can thus be formed from the different species impinging on the surface, that is, ions, radicals, and neutral monomers, and reacting with each other, forming interconnected random-like structures.^[6,8,9] Due to the large number of species on the plasma-exposed surfaces, it is often difficult to identify the specific species responsible for the growth of the C:H film. This is especially true since the synergistic interaction of different species can strongly influence the growth process (e.g., the synergy between CH₃ radicals and ions impinging on the surface has been shown to increase the contribution of these radicals to film growth^[10,11]) and the exact composition of the species flux depends strongly on external discharge parameters such as pressure, power, gas flow rate, and so on. The role of the different radicals and the contribution of ions to the growth process are the subject of active discussions in the scientific community. Ions accelerated in the sheath have significant kinetic energy and can initiate reactions and bond breaking. Consequently, they can determine whether films grow in a “soft” form (polymers) under low ion energies or in a “hard” form with extensive cross-linking under high-energy ion bombardment.^[6,7] Numerous experimental studies show the importance of radicals in the growth of hydrocarbon films.^[12–15] Their contribution to film growth can be investigated by estimating their respective surface loss probabilities.^[11,16] Due to the complexity of the plasma process, which involves numerous gas-phase and surface reactions, the manufacture of a tailor-made thin film for a particular application remains a major challenge in the field. It is, therefore, clear that mastery of the deposition technique can only be achieved through a fundamental understanding of the chemical and physical phenomena involved in film formation.

Accordingly, this study aims, first, to understand the mechanisms of hydrocarbon film growth on a surface involving the main neutral species (CH₄, C₂H₄, C₂H₂, C₂H, CH₃, and H₂) of an Ar/CH₄ low-pressure plasma at temperatures of 300, 400, 500, and 1000 K. These species are derived from a first-dimensional (1D) fluid model used to simulate the electronic impact processes on the monomer gas for

C₂H₂^[17,18] and for CH₄.^[19] For simplicity, the 1D fluid code is modeled only at 300 K and temperature variation is performed during molecular dynamics (MD) simulations, recognizing that temperature variation in the 1D fluid model could have produced slightly different species distributions. The current temperature range is considered typical for capacitively coupled radiofrequency discharges, which typically operate at 300–400 K.^[20] Temperatures of up to 1000 K are also considered to evidence temperature effects, since methane is an interesting molecule for diamond deposition, which requires a higher gas temperature, even higher than 1000 K.^[21] Second, the influence of major ions (Ar⁺ and C₂H₃⁺) from the Ar/CH₄ plasma on the C:H film is studied at energies of 50, 75, and 100 eV. These energies were chosen because they belong to the energy range relevant for plasma deposition (25–500 eV).^[5]

This paper is organized as follows: In the next section, we present the details of the calculations, namely, the MD simulation method, the input data, and the different simulation protocols. In Section 3, we first present the structures of the films formed at different temperatures, determine the total deposited mass, and then discuss the different contributions of each incident species to the growth. The C:H films are then characterized by determining the different bond types and coordination numbers (CNs) between the carbon atoms. The separate bombardment of the C:H film with different ions is then discussed by determining its mass evolution due to ion impacts. It should be pointed out that the present work yields molecular scale-level knowledge. It is also interesting to note that this study highlights the process involved rather than assuming some of them like in fluid models.

2 | COMPUTATIONAL DETAILS

2.1 | MD

Classical MD is a computer simulation method that is used to calculate the evolution of a system of atoms over time by solving Newton's equations of motion over many discrete time steps. At each time step, the forces exerted on all atoms by all other atoms are calculated, and the velocities and positions are updated.^[22,23]

$$\vec{F}_i(t) = m_i \frac{d^2 r_i(t)}{dt^2} = \sum_{\substack{j=1 \\ j \neq i}}^N \vec{F}_{j \rightarrow i}(t), \quad (1)$$

$$\forall i \in \{1, \dots, N\}.$$

The force field acting on the system is conservative in nature. This means that the forces \vec{F}_i can be obtained from the gradient of the potential energy U of the system as a function of the interatomic distances.

$$\vec{F}_i(t) = -\vec{\nabla}_i U(\vec{r}_1, \vec{r}_2, \vec{r}_3, \dots, \vec{r}_N). \quad (2)$$

The temporal resolution of Equation (1) requires knowledge not only of the initial positions and velocities but also of the potential energy or interatomic potential of the system. Since our study system is defined by the interaction of the atoms of hydrocarbon molecules with an initial Fe₆₇Cr₁₇Ni₁₄Mo₂ stainless-steel surface, the interatomic potential of the system can be described by the expression:

$$U_{\text{system}} = U_{\text{HC}} + U_{\text{surf}} + U_{\text{HC-surf}}, \quad (3)$$

where U_{HC} is the interatomic potential describing the C–C, C–H, and H–H interactions, U_{surf} is the interatomic potential describing the interactions between the substrate atoms (Fe, Cr, Ni, and Mo), and $U_{\text{HC-surf}}$ is the interatomic potential describing the interactions of the atoms of the incident species with those of the substrate.

The Reactive Empirical Bond Order (REBO)^[24] potential is used in our study to describe U_{HC} .^[4,6,19] Zarshenas et al.^[6] compared different reactive hydrocarbon potentials, namely, REBO, Adaptive Inter-molecular Reactive Empirical Bond Order,^[25,26] Reactive Force Field,^[27] and Charge Optimized Many Body^[28,29] with results from Density Functional Theory in order to select the best potential for studying reactions leading to the growth of hydrocarbon polymers on a silver substrate. The authors found that the REBO potential is best suited to describe U_{HC} because it did not present any reaction energy barrier to polymer formation on the surface. In addition, this potential is commonly used in the literature^[4,6,30–33] to describe U_{HC} and is faster than other hydrocarbon potentials.^[34] It should be noted that the distinction between radical and nonradical hydrocarbon species in our MD simulations is based on the concept of bond order of the REBO potential. It is important to note that this potential does not include charged particles. However, in the present work, ions are treated as neutral species with high kinetic energy impinging on the surface.

U_{surf} interactions have been described using the embedded atom method potential,^[35–38] which is an ideal method for describing metals and metal alloys. To describe $U_{\text{HC-surf}}$, we used the Lennard–Jones (LJ) potential.^[4,39] The LJ potential is generally inadequate for simulations involving the growth of hydrocarbon films on a stainless-steel surface. While it can capture

certain aspects of van der Waals forces and short-range repulsion, it does not allow the modeling of a reactive system (e.g., the growth of hydrocarbon films). For this reason, we have used the REBO potential to allow surface reactions between hydrocarbon species and the LJ potential to describe nonbonding pair interactions between the atoms of stainless-steel and those of the incident molecules.

Newton's equations were integrated using the open source code Large-scale Atomic/Molecular Massively Parallel Simulator.^[40] Visual Molecular Dynamics^[41] and OVITO^[42] software were used to visualize the MD simulation results and Python scripts were written for data processing.^[43] Five simulations were performed for each parameter considered (temperature and energy) in order to obtain statistically reliable results.

2.2 | Simulation method

The initial species considered in our study were derived from a 1D fluid model of the Ar–4%CH₄ mixture^[17–19] reflecting experimental conditions.^[44] The reference conditions of the 1D fluid model are summarized in Table 1, and the species resulting from this model (main neutrals and ions in the sheath) are shown in Table 2.

MD simulations are carried out with the aim of forming a hydrocarbon film on the surface by injecting species at temperatures of interest. The grown film structure is then characterized and the species contributing to their growth are identified. First, MD simulations are performed by sending all the main neutral species (49 600 molecules in total) to a stainless-steel surface [composed of 67% iron (Fe), 17% chromium (Cr), 14% nickel (Ni), and 2% molybdenum (Mo)], taking into account the molar fraction of each species (Figure 1a and Table 2). These

TABLE 1 Reference data of the one-dimensional fluid model from which the input data of our study are derived.

Reference conditions	
Temperature	300 K
Pressure	70 Pa
Vrf	100 V
Frequency	13.56 MHz
Interelectrode distance	2.54 cm
Secondary electron emission yield	0.01
Percentage of argon	96
Percentage of methane	4

species are sequentially sent to the surface at a rate of one molecule every 500 fs over a total simulation time of 26 ns (using 800 species injection cycles as displayed in Figure 1a), to create competition between species to mimic the experiments. The initial velocities of these incident species and those of the substrate are randomly selected from a Maxwell–Boltzmann distribution at temperatures of

TABLE 2 Main neutral species and ions in the sheath resulting from the 1D fluid model used as input for MD simulations.

Main neutral species	Molar fractions	Main ions in the sheath	Molar fractions
H ₂	3.20×10^{-2}	Ar ⁺	1.40×10^{-8}
CH ₄	1.40×10^{-2}	C ₂ H ₃ ⁺	1.30×10^{-8}
C ₂ H ₄	5.40×10^{-3}	ArH ⁺	7.00×10^{-9}
C ₂ H	3.20×10^{-3}	C ₂ H ₅ ⁺	5.70×10^{-9}
C ₂ H ₂	2.70×10^{-3}	C ₂ H ₂ ⁺	3.80×10^{-9}
CH ₃	2.30×10^{-3}	C ₂ H ₄ ⁺	3.50×10^{-9}
		CH ₃ ⁺	2.30×10^{-9}
		H ₂ ⁺	1.60×10^{-9}
		CH ₄ ⁺	1.10×10^{-9}

Note: Neutral argon is not included in our simulations.^[19]

Abbreviations: 1D, one-dimensional; MD, molecular dynamics.

300, 400, 500, and 1000 K. The stainless-steel substrate with a size of $4.018 \times 4.018 \times 4.018 \text{ nm}^3$ contains 1960 atoms and is divided into three zones (Figure 1a): the fixed zone to maintain the structure of the substrate and the stochastic zone, where a Langevin thermostat with a relaxation time of 10 fs was applied for dissipating the energy diffusing from the reaction zone, where interaction occurs between the incident species and the substrate atoms. In a second step, the same procedure as in Figure 1a was applied, including the two main ions Ar⁺ and C₂H₃⁺ (Figure 1b) from Table 2 to study the effect of these ions on film growth. The ion injection consists of the injection of one ion (randomly selected from two ions, with a velocity of $\vec{v}_{ion} = \sqrt{2E/m} \vec{e}_z$ at an energy of 50 eV) after a complete neutral injection cycle, as shown in Figure 1b.

To evaluate the role of ions, we determined several parameters such as the H/C ratio, the total deposited mass, and the contribution of each species to C:H film growth over time at different temperatures for simulations with and without ions. We observed an overlap in the curves for the different parameters between simulations with and without ions (the curves are not shown here), suggesting that the influence of ions at 50 eV during C:H film growth is not significant. Moreover, the ions are present in very small amounts in our simulations compared to the

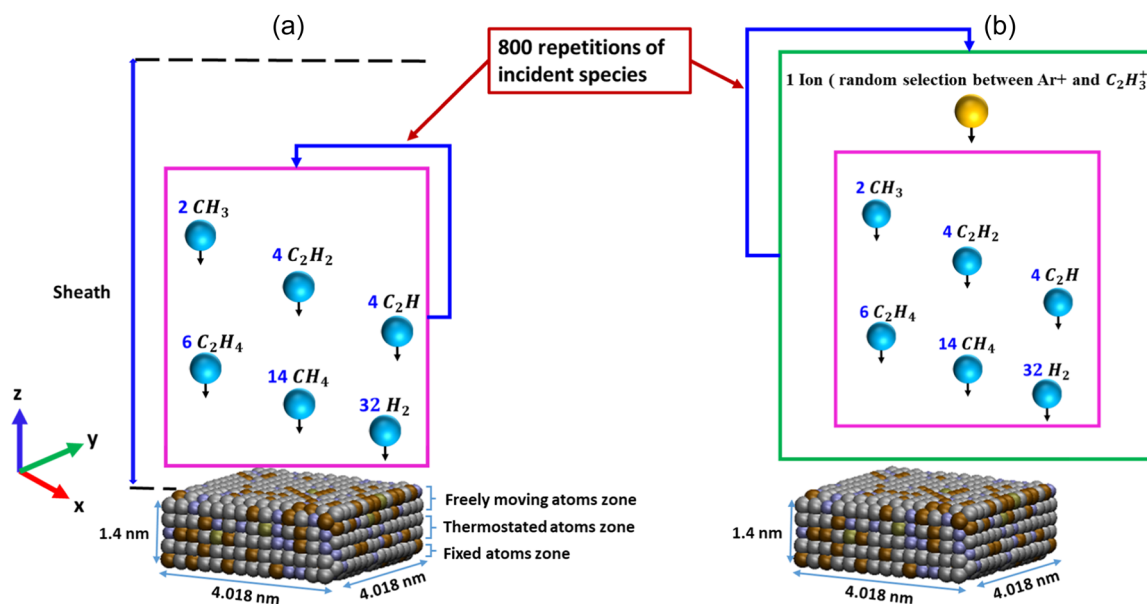


FIGURE 1 Schematic representation of the initial arrangement of the system for sending all neutral species together (a) and with the inclusion of ions (b). In both cases, the cells framed in pink represent the deposition of one cycle of neutrals repeated 800 times. These species are sent toward a stainless-steel plate composed of 67% Fe (silver color), 17% Cr (ocher color), 14% Ni (glacier blue color), and 2% Mo (tan color).

neutral species (of the order of 0.08%), which also justifies their insignificant contribution or influence during C:H film growth. Therefore, in the following sections, the initial growth of C:H films is considered without the ion contribution, as shown in Figure 1a at temperatures of 300, 400, 500, and 1000 K. The possible role of ion bombardment on a grown film will be studied separately for different energies in Section 3.4.

3 | RESULTS AND DISCUSSION

3.1 | Total deposited mass and the H:C ratio of C:H films

In this section, we describe the different C:H films formed after 26 ns of simulation when all neutral species were sent together to the surface (Figure 1a) at different temperatures. Figure 2a shows three-dimensional views of these C:H films at temperatures of 300, 400, 500, and 1000 K. A first obvious observation is that these films have an “amorphous” morphology. To further characterize these films, we first determined the corresponding total mass of the C:H films (Figure 2b). The mass remains constant up to a temperature of 500 K and decreases by around

10% at 1000 K. This behavior is due to the fact that the substrate atoms move little at low temperatures (300–500 K), which makes the sticking of the incident species easier. When the temperature (of the substrate and the incident species) increases above 1000 K, the thermal excitation of the substrate atoms and the high velocities of the incident species prevent certain molecules from sticking to the substrate.

The relative abundance of hydrogen and carbon atoms in the C:H film is of particular importance (Figure 2c). It provides an indication of the type of bond between carbon atoms that predominates in the C:H film. Indeed, a high H:C ratio (closer to 2) indicates a high degree of saturation (i.e., predominance of single bonds between carbon atoms), while a low H:C ratio (close to 1 or below) indicates a high degree of unsaturation (i.e., predominance of double or triple bonds between carbon atoms).

It can be seen that the H:C ratio of the C:H films (Figure 2c) ranges from 0.6 to 0.7 at all temperatures, where the temperature dependence of the ratio is similar to that of the total deposited mass, with less hydrogen sticking at 1000 K than at other temperatures. These different values indicate that the C:H films contain considerably more carbon atoms than hydrogen atoms and that there are more double or triple bonds between carbon atoms at all temperatures.

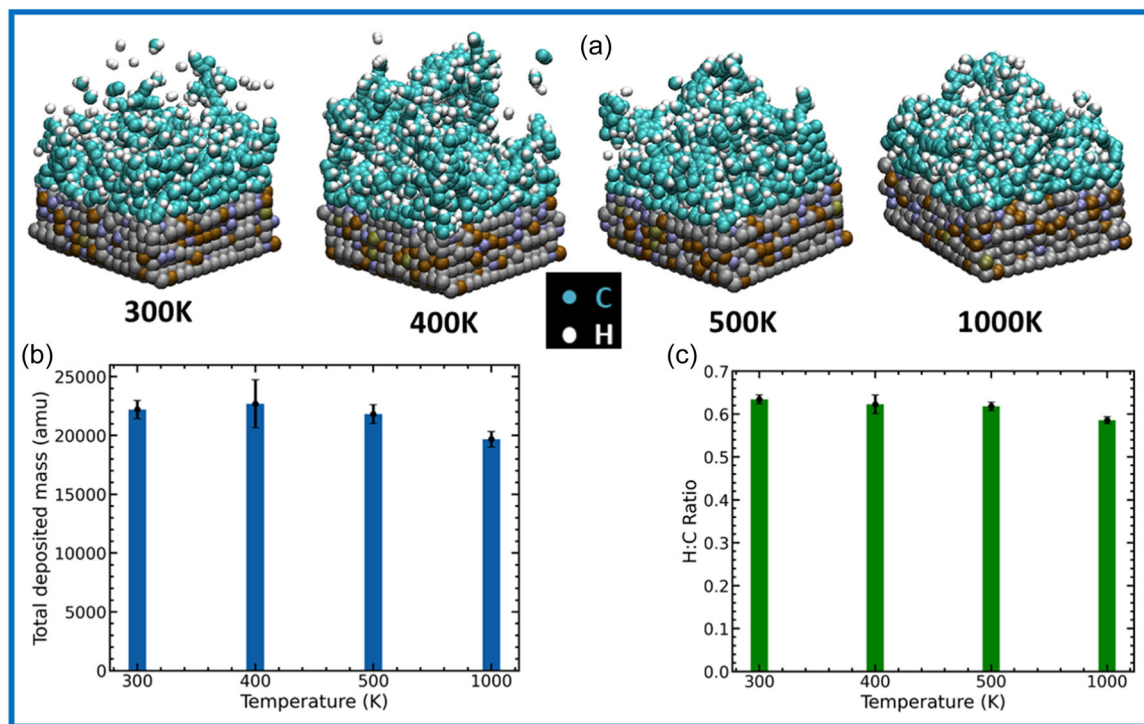


FIGURE 2 Three-dimensional view of the C:H films formed after 26 ns when neutral species are deposited together on the surface (a), the total deposited mass (b), and the H:C ratio of the C:H films (c) as a function of temperature.

3.2 | Contribution of each initial species to the growth of C:H films

In a first step, we determined the global sticking coefficient (GS) during film growth; this is defined by the following equation as follows:

$$GS = \frac{N_{\text{stuck}}(\text{whatever the species, with } z \leq z_c)}{N_{\text{incident}}}, \quad (4)$$

where N_{stuck} and N_{incident} are the total number of molecules stuck to the surface and the total number of incident molecules from the initial step of the simulation to time t , respectively; z_c is the critical height, above which there are no more bonded atoms/molecules on the growing film. All species with $z > z_c$ are considered as reflected. The temporal evolution of the GS is shown in Figure 3 at different temperatures.

It can be seen that the GS is maximum (~ 0.7) in the first instants of the simulations (between 0 and 1 ns) and then quickly decreases with time, reaching a constant value of about 0.05 after 5 ns. This suggests that the sticking is favored when the surface is pristine and tends to drastically decrease with film growth.^[16] However, despite this small sticking coefficient, the film is able to grow as shown in Figure 2. At 1000 K, the GS is much smaller when the surface is pristine. This shows that several species contributing to film growth on the pristine surface at lower temperatures can no longer stick at higher temperatures. To better understand this behavior, the contribution of each species to film growth has to be investigated as a function of time.

These contributions were determined using the following relationship:

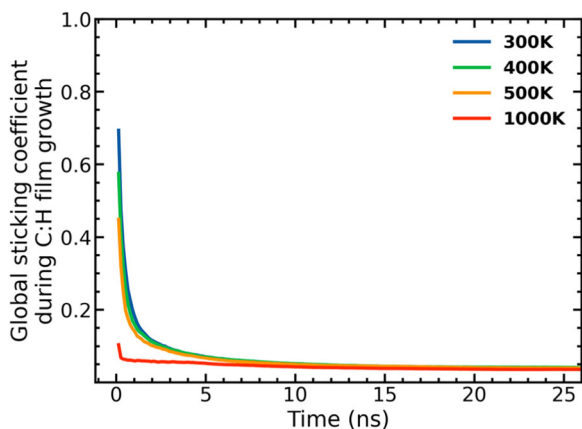


FIGURE 3 Global sticking coefficient of all incident neutral species during C:H film growth at temperatures of 300, 400, 500, and 1000 K.

$$\text{Fractional contribution (\%)} = \frac{m_x}{m_d} \times 100, \quad (5)$$

where m_x is the mass of the considered neutral incident species and m_d is the total deposited mass.

Figure 4-d show the contribution of the incident neutral species to the growth of the C:H film over time at temperatures of 300, 400, 500, and 1000 K, respectively.

At all temperatures, except for H_2 , which is fully reflected, the contributions of stable (not very reactive) species such as CH_4 , C_2H_2 , and C_2H_4 reach a maximum value in the first instants (between 0 and 1 ns) before decreasing rapidly in the case of CH_4 and C_2H_4 and slowly in the case of C_2H_2 as the C:H films grow. This behavior indicates that these stable species contribute significantly to the formation of the first C:H layer during the first instants. When the surface is pristine, these nonreactive species are able to stick on the stainless-steel surface. After the first C:H monolayer is formed, they are almost completely reflected, unable to create bonds with deposited hydrocarbon species.

The behavior of these stable species is consistent with the time evolution of the GS at all temperatures (Figure 3), with the high values in the first instants justified by the contributions of the stable species C_2H_2 , CH_4 and C_2H_4 . The decrease in the maximum values (in the first instants) of the GS as the temperature increases is consistent with the fractional contribution of CH_4 , which also decreases with increasing temperature. Since the number of CH_4 molecules is much higher than that of other neutral species, if it no longer sticks, the GS drastically decreases. Thus, the CH_4 sticking behavior explains the temperature and temporal evolutions of the GS.

For the radicals, we observe that at all temperatures, the contribution of C_2H increases with time, while that of CH_3 is nearly zero. This indicates that the C_2H radical is the main precursor of C:H film growth. The overall results observed after the formation of the first C:H layer are consistent with the observations described in Jacob's review paper,^[5] in which it is reported that nonradical neutral species such as CH_4 , C_2H_2 , C_2H_4 , and H_2 do not contribute to the growth of C:H films and that the contribution of CH_3 is negligible, as this radical is more volatile (i.e., less reactive) than C_2H . Therefore, it is assumed that the growth of C:H films is driven by radical species (mainly C_2H) and that stable species are generally fully reflected after interaction with the surface.^[5,17,45,46] Moreover, using MD simulations, Sharma et al.^[47] observed that stable species (CH_4 , C_2H_2 , C_2H_4 , and H_2) had a 100% chance of being fully reflected after interacting with an amorphous carbon surface at low energies (below 0.75 eV), an observation also made by

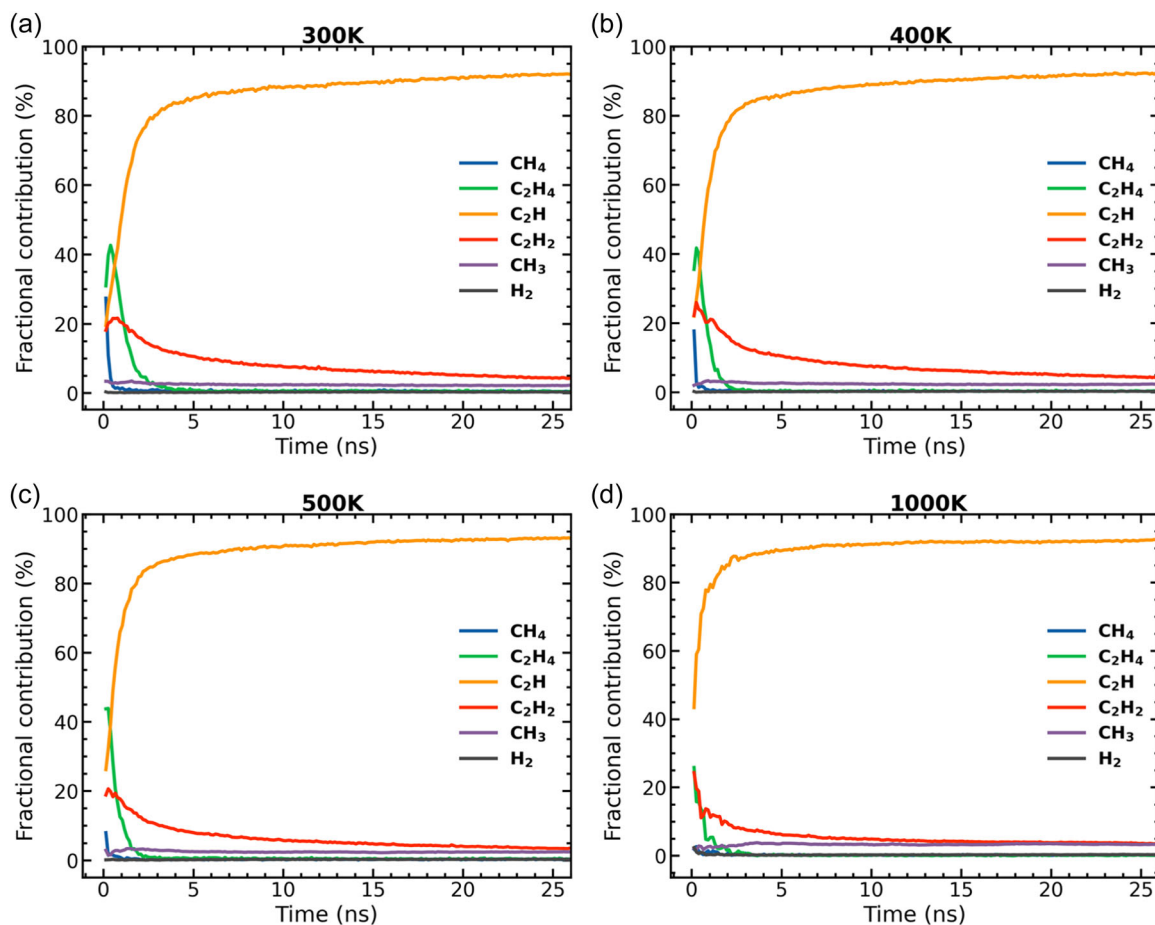


FIGURE 4 Fractional contributions of major neutral species in Ar/CH₄ plasma to the growth of C:H films at temperatures of 300 (a), 400 (b), 500 (c), and 1000 K (d).

Alman and Ruzic^[48] in their work on calculating the reflection and dissociation coefficient of hydrocarbon species. In accordance with these results, our study also highlights that stable hydrocarbon species play an important role in the formation of the first C:H layer when the surface is pristine.

It should be noted that the contribution of the CH₃ radical to the growth of the C:H film depends on the availability of dangling bonds at the surface. These dangling bonds can be created or enhanced by the flux of atomic hydrogen or ions impinging on the surface.^[11,49] Simultaneous ion bombardment leads to an increase in the contribution of CH₃ to C:H film growth due to synergy between ion bombardment and radical incorporation.^[5,11,13] As described in Section 2.2, we also performed MD simulations in which the ions were considered as high-velocity neutral particles (Figure 1b). However, in our conditions, these ions are present in very small amounts compared to the incident neutral species and they do not significantly affect the species contributions to the growth of the C:H films. In fact, MD

simulations carried out with the inclusion of the two main ions showed that the contributions of the individual species to film growth are practically the same as in Figure 4.

Contrary to CH₃, the C₂H radical does not require a specific adsorption site on the surface to chemisorb due to its high reactivity.^[15] This radical is widely known for its important role in the growth of C:H films on the surface also in acetylene-based discharges.^[45,50,51]

The reactivity of a radical species is a key parameter for the growth of C:H films.^[1] Although the more reactive radicals are the predominant ones contributing to the growth of CH films, the less reactive radicals such as CH₃ can also play an important role in surface reactions. They can be involved in the formation of volatile species during the growth of C:H films, as shown for CH₃ in our previous work.^[16] The direct consequence of this interaction of CH₃, and other molecules, with the surface is that the surface can change the global chemistry of the surrounding plasma by removing some species from the gas phase and by acting as a source of

new molecular species. To date, this aspect has not been satisfactorily considered in existing studies due to its high complexity.

3.3 | Characterization of deposited C:H films

3.3.1 | Bonds between carbon atoms in the C:H films

To characterize the formed C:H films, we determined the bond types of the carbon atoms in the film at all temperatures thanks to the radial distribution function (RDF) calculated at 26 ns (Figure 5a). RDF is a mathematical concept that describes the distribution of distances between particles in a system.

Depending on the distance between carbon atoms, the peaks (from left to right) correspond to triple (C≡C), double (C=C), and single (C–C) bonds. By integrating the area of these peaks, the respective proportion of the different bond types is determined (Figure 5b). It can be seen that the C:H films are dominated by C=C double bonds at all temperatures. This indicates that the films are relatively unsaturated, which is consistent with the H:C ratio values obtained in Section 3.1. The presence of these bonds decreases significantly at 1000 K, while C–C single bonds are increasing. This means that high temperatures increase the molecular motions of impinging species, causing strong bonds (such as C=C or C≡C) to be broken to form single ones with other surface carbon atoms when they collide with the surface. However, as for triple bonds (C≡C), their percentage remains relatively small. Since the C₂H radical is the main contributor to the growth of C:H films at all

temperatures, it indicates that a large fraction of the C≡C triple bonds of this radical is converted into double bonds (C=C) during sticking to the surface.

3.3.2 | CN of carbon atoms in C:H films

The CN of carbon atoms in C:H films is defined as the number of nearest-neighbor atoms (C or H) of each carbon atom:

$$\text{CN}^x = \frac{N_x}{N_c} \times 100, \quad (6)$$

where N_x is the number of carbon atoms with CN^x (i.e., $x=2$ or 3 or 4) and N_c is the total number of carbon atoms in the film. Figure 6a shows the CN of the carbon atoms CN^2 , CN^3 , and CN^4 as a function of temperature. The notation used here is analogous to that of Zarshenas et al.^[6]

It can be seen that CN^3 carbons (yellow dash line) dominate (about 65%) and that their number increases slightly with increasing temperature. This is consistent with the dominance of double bonds in the C:H films observed in Section 3.3.1. Indeed, carbon atoms generally form only four covalent bonds to satisfy their valence (corresponding to a CN of 4). When a carbon atom forms a C=C double bond with another carbon atom, it loses one more potential bonding site compared to forming a single bond. The two atoms in the double bond share two of their valence electrons in a σ bond and two electrons in a π bond, leaving them with two electrons each to form either two single bonds or a double bond with other atoms. This results in a coordination geometry that justifies the number of CN^3 carbon atoms observed.

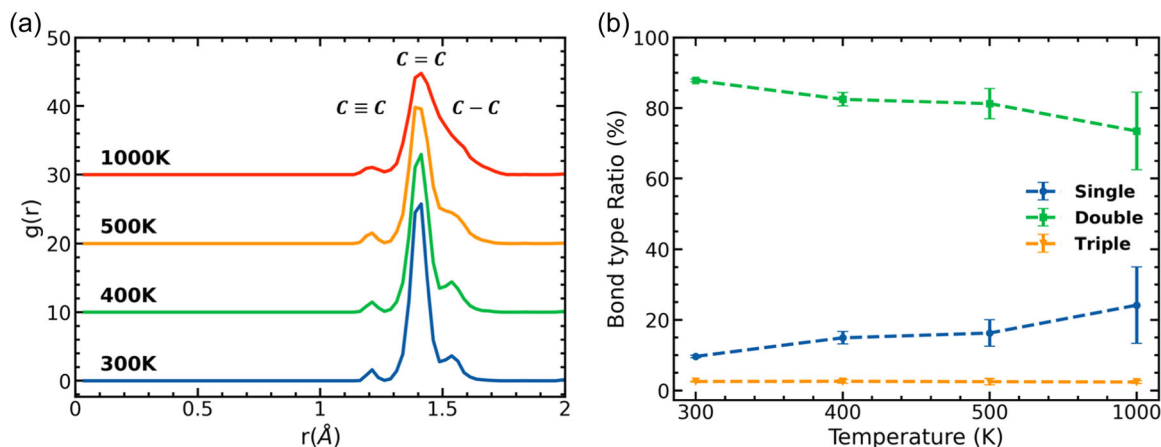


FIGURE 5 (a) Radial distribution function between carbon atom pairs in the C:H films and (b) respective proportion of bond types at 300, 400, 500, and 1000 K.

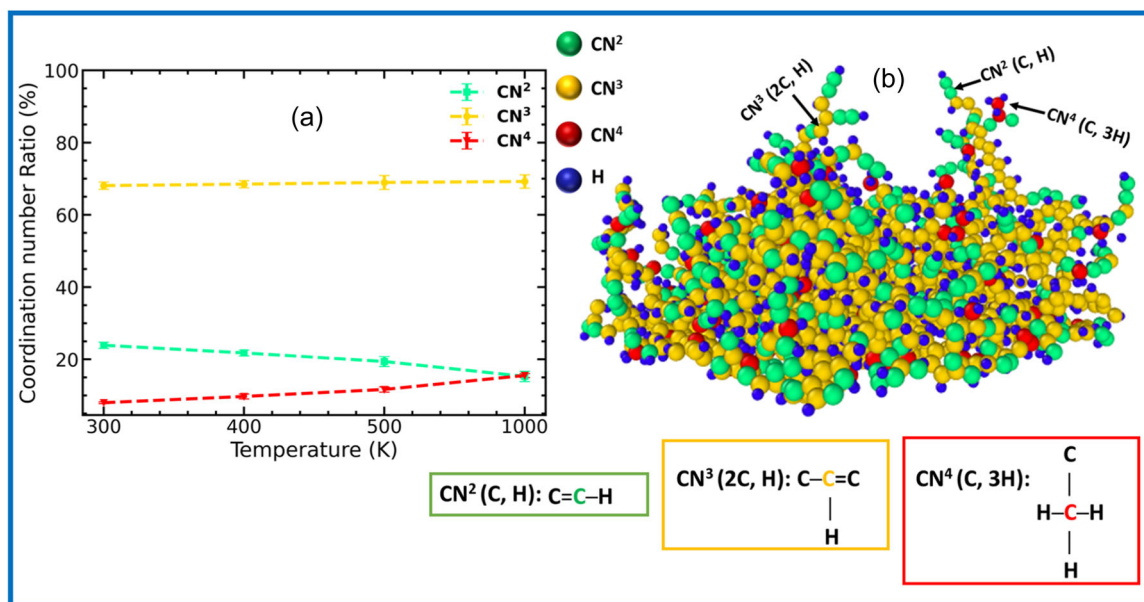


FIGURE 6 (a) Coordination number (CN^2 , CN^3 , and CN^4) of carbon atoms in C:H films as a function of temperature and (b) snapshot highlighting CN^2 , CN^3 , and CN^4 carbon atoms and hydrogen atom (H) at 300 K. The major configuration of each CN^x is shown in the corresponding colored boxes, where the colored carbon atom is the corresponding CN^x carbon.

The slight increase in CN^3 as a function of temperature can be explained by the behavior of the C_2H radical, which is the main precursor of C:H film formation at all temperatures. This means that it specifically promotes the formation of CN^3 carbons, which become slightly more important at higher temperatures as the stable neutral species contribute less significantly at high temperatures (see Figure 4, at the first instant of the simulations).

Considering the abundance of carbon atoms relative to hydrogen atoms and the different visualizations performed during postprocessing using OVITO software, we also found that the main CN^3 carbon configuration is $\text{CN}^3(2\text{C}, \text{H})$, that is, one CN^3 carbon atom is bonded to 2C atoms and 1H atom. This main configuration of CN^3 atoms is shown in the yellow box in Figure 6b, which is a snapshot highlighting the CN^x carbons atoms in the C:H film at a temperature of 300 K (other temperatures are not shown here). For the CN^2 carbons (green dashed line), we find that their number is larger at low temperatures and decreases with increasing temperature, favoring an increase in CN^4 carbons (red dashed line). This is because higher temperatures can lead to increased mobility of atoms and molecules within the C:H films. This increased surface mobility can promote molecular rearrangements that lead to the formation of additional carbon-carbon bonds, increasing the CN of certain carbons to CN^3 or CN^4 . The decrease in CN^2 carbons with increasing temperature could also be attributed to the higher activation energy required to maintain the

bonds at higher temperatures. CN^2 carbon bonds could be less stable with increasing temperature, leading to a decrease in their quantity.

As noted in Section 3.3.1, triple bonds $\text{C}\equiv\text{C}$ are negligible compared to other bonds, so double bonds also dominate the configurations of CN^2 carbon atoms, as shown in the green box in Figure 6b. In contrast, the CN^4 carbon atoms contain only single bonds with their nearest neighbors. We estimated that the major configuration of CN^4 atoms is $\text{CN}^4(\text{C}, 3\text{H})$, as shown in the red box in Figure 6b.

It should be noted that here, we have presented only the configurations of CN^x carbon atoms that we have assumed to be in the majority, based on the various visualizations. However, CN^x carbon atoms can have other configurations and these can change significantly with temperature variations, but this aspect is not addressed in our work.

3.4 | Ar^+ and C_2H_3^+ ion bombardment of the C:H film

The bombardment of the surface by energetic particles plays a crucial role in the plasma-surface interaction. Indeed, the interaction of, for example, hydrocarbon ions with the surface is important as these ions can contribute to film growth, and the impact of Ar^+ ions can lead to the formation of “hard” hydrocarbon films by energy transfer from the incident ions to the film.^[5]

In this section, we have performed MD simulations to study the bombardment of the C:H film by Ar^+ and C_2H_3^+ ions at different energies (50, 75, and 100 eV). These ions are the two main ions formed in the Ar/ CH_4 plasma modeled by the 1D fluid model (Table 2) and are treated as high-velocity neutral species in our study. Although the absence of ionic charges means that there are no direct Coulombic interactions between ions and surface atoms, high-velocity neutral particles can transfer momentum to the atoms of the C:H film upon impact. This momentum transfer can lead to the ejection of surface atoms and molecules or to changes of the film structure. Indeed, the absence of charge does not preclude the possibility of bond breaking and bond formation during ion impact. These simulations are useful to determine the mass change of the film under

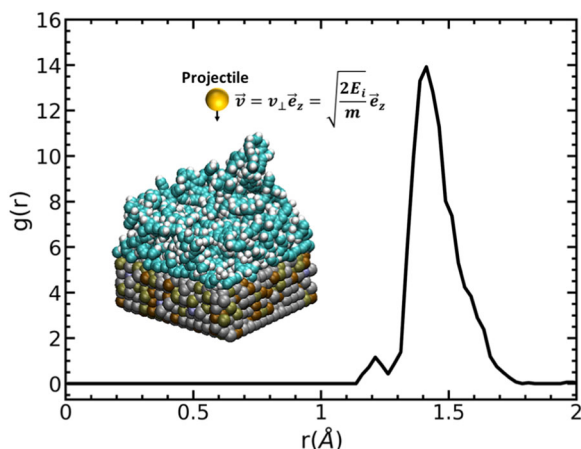


FIGURE 7 Initial model of a C:H film (with its radial distribution function) to be separately bombarded with Ar^+ or C_2H_3^+ ions at energies of 50, 75, and 100 eV. This film, resulting from the deposition of all neutrals at a temperature of 300 K, was relaxed at 300 K before ion bombardment.

nonreactive (Ar^+) and reactive (C_2H_3^+) ion bombardment. The bombarded C:H film (Figure 7) is the one formed at a temperature of 300 K (Figure 2a) by the global deposition of neutral species (Figure 1a). Unbounded atoms in the C:H film formed at 300 K (see Figure 2a) were first removed, then the film was relaxed over a short simulation time of 1 ps before ion bombardment at 300 K to obtain a more stable and compact structure (as shown in Figure 7), to avoid our C:H film being completely pulverized in the very first instants of the simulation (since our films are soft). This relaxation led to a rearrangement of the bonds between the carbon atoms in the film, as shown by the RDF of the film in Figure 7.

The initial C:H film contains a total of 2623 atoms with an H:C ratio of about 0.56. A total of 1000 ions of each species are sent toward the film with a time step of 0.1 fs, at a rate of one ion every 5000 time steps, that is, 500 fs between two impacts and a total simulation time of 500 ps. Figure 8a,b shows the evolution of the mass of the C:H film as a function of the number of Ar^+ and C_2H_3^+ ion impacts for the different energies considered.

At 50 eV, a very small (negligible) mass change is observed with the impacts of Ar^+ ions, regardless of the number of impacts. On the other hand, at the same energy, an approximately linear increase in the mass of the C:H film is observed upon the impact of C_2H_3^+ ions. These different observations are directly related to the evolution of the H:C ratio as a function of the number of impacts during bombardment by Ar^+ (Figure 9a) and C_2H_3^+ (Figure 9b) ions. This indicates that Ar^+ ions, at this energy, do not significantly affect the chemical composition of the film, while C_2H_3^+ ions change this composition by introducing carbon and hydrogen atoms into the C:H film. C_2H_3^+ ions are reactive species whose sticking coefficient at room temperature is considered to

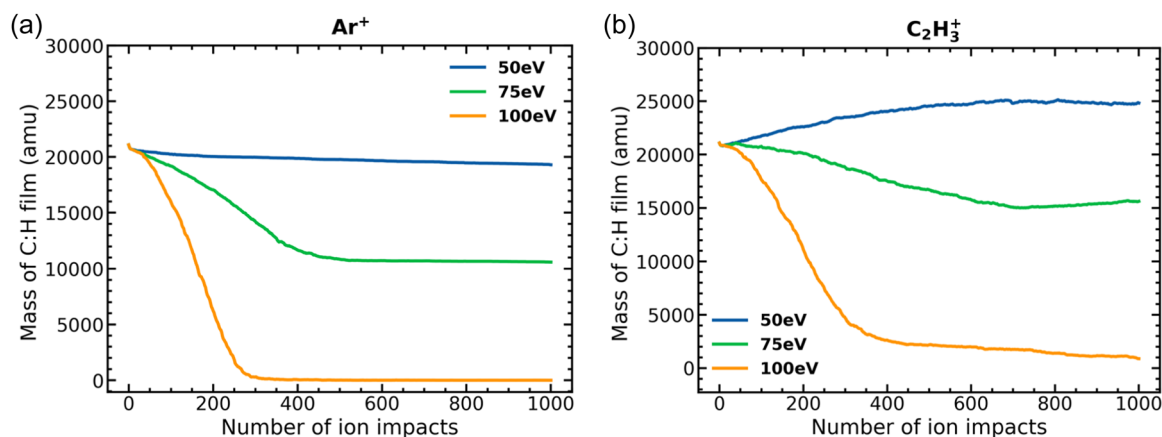


FIGURE 8 Evolution of the mass of the C:H film as a function of the number of impacts of Ar^+ ions (a) and C_2H_3^+ ions (b) at energies of 50, 75, and 100 eV.

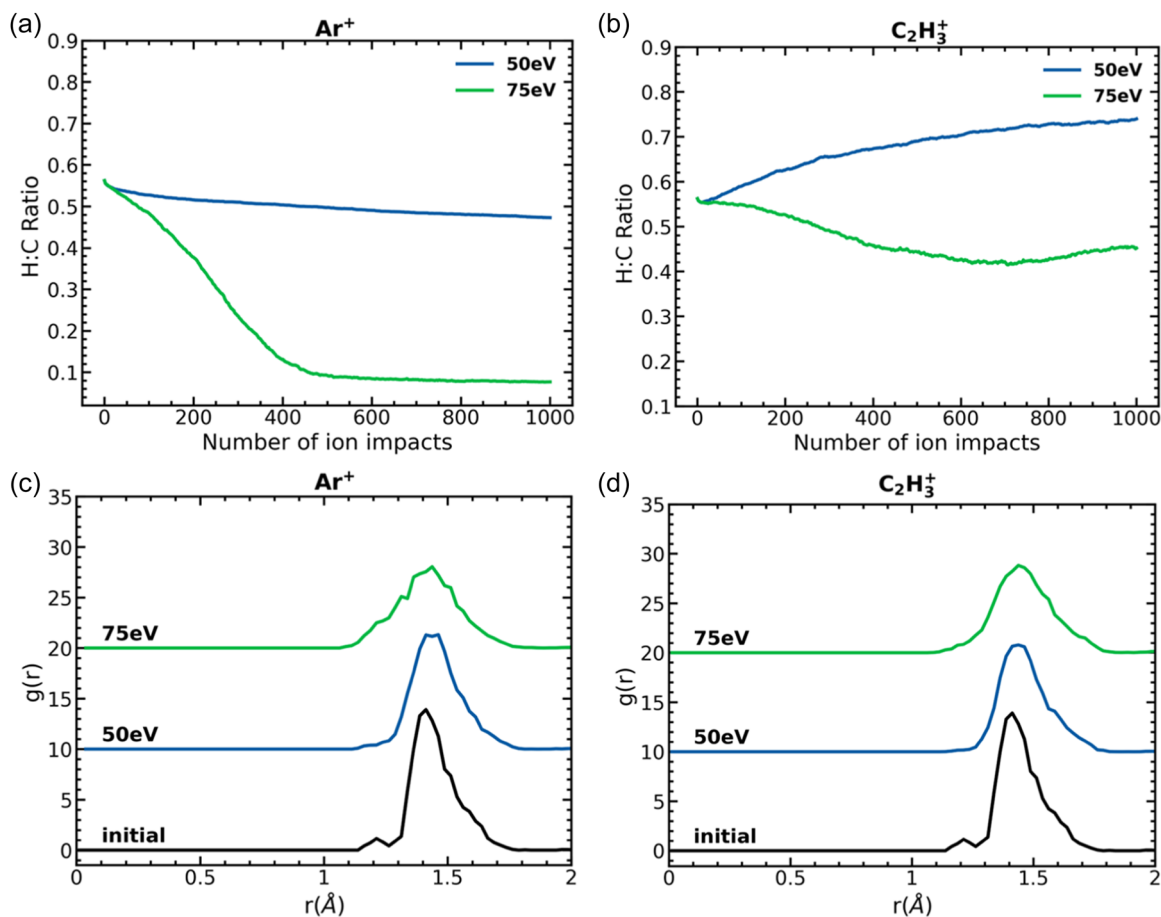


FIGURE 9 Evolution of the H:C ratio as a function of the number of Ar⁺ (a) and C₂H₃⁺ (b) ion impacts and the radial distribution functions (RDFs) between the carbon atom pairs of the initial and final C:H films after bombardment by Ar⁺ ions (c) and C₂H₃⁺ ions (d) at energies of 50 and 75 eV. The H:C ratio and the RDF at 100 eV are not shown because at this energy, the C:H film is completely sputtered after bombardment by Ar⁺ ions and only a small mass of the C:H film remains after bombardment by C₂H₃⁺ ions.

be equal to 1.^[52,53] When these ions impact the C:H film at higher energy (such as 50 eV), they can undergo chemical reactions with the hydrocarbon molecules of the film. These reactions can incorporate carbon and hydrogen atoms from the ions into the C:H film, increasing the mass of the film, as shown in Figure 8b (blue curve). These observations also indicate that an energy of 50 eV is not sufficient for Ar⁺ or C₂H₃⁺ ions to significantly sputter the C:H film at the surface.

Although the C:H film is not significantly sputtered after ion impact at 50 eV, a reorganization of the film atoms can be observed from the final RDFs of the C:H film after Ar⁺ ion impact (Figure 9c, blue curve) and C₂H₃⁺ ion impact (Figure 9d, blue curve) compared to the initial C:H film structure. We can see that the Ar⁺ ion impact and the C₂H₃⁺ impact at 50 eV have reorganized the C:H film such that the film contains almost no C≡C triple bonds between carbon atoms.

At 75 eV, it can be seen from Figure 8 (a green curve) that the mass of the C:H film gradually decreases during

the first few impacts (between 0 and 400 impacts) of Ar⁺ ions, followed by stabilization. The mass decrease is due to the sputtering effect leading to bond breaking and ejection of C and H atoms from the surface, as also shown by the evolution of the H:C ratio (Figure 9c, green curve) at these same impact times. The rapid decrease in the H:C ratio indicates that C–H and H–H bonds are the ones that can be easily broken by Ar⁺ ions to eject a hydrogen atom. The mass stabilization after about 400 impacts may be due to a reorganization of the film under the influence of the ion impacts, leading to a more stable and compact configuration that can withstand further sputtering. This is confirmed by the final H:C ratio, which is very low (about 0.1), meaning that the film contains only a very small amount of hydrogen and the remaining film is therefore strongly dominated by bonds between carbon atoms. In addition, we determined the CN of carbon atoms in this film (figure not shown here) and CN³ carbon atoms predominate (about 75%) in the final film, indicating from the value of the H:C ratio that

the CN^3 (3C) configuration, that is, one carbon atom bonded to three carbon atoms, is the most dominant. This is confirmed by the RDF of the final C:H film (Figure 9c, green curve), which seems to show that there are more C–C single bonds than double and triple bonds. These observations indicate that the CN^3 (3C) structures in the C:H film are difficult to break.

On bombarding the C:H film by $C_2H_3^+$ ions at 75 eV (Figure 8b), we observe a weak decrease in the mass of the C:H film, which is due to the fact that there is competition between sputtering and incorporation of atoms from incident ions into the film (due to the reactive nature of $C_2H_3^+$), justified by the evolution of the H:C ratio (Figure 9b, green color). This leads to simultaneous bond breaking and bond formation phenomena, with C=C double bonds largely dominating as shown in the RDF of the final C:H film (Figure 9d, green curve). The slight increase in the mass of the C:H film from about 700 impacts of $C_2H_3^+$ ions shows that from this moment, the formation of bonds between the atoms of the ions and those of the film dominates over the sputtering. This is probably due to the rearrangement of the surface atoms during the bombardment, which leads to bonds in the film that are difficult to break.

Finally, at 100 eV, the C:H film is completely sputtered after 300 Ar^+ ion impacts (Figure 8a, orange curve). Ar^+ ions impacting the film at high velocities break bonds and eject atoms from the film. For the $C_2H_3^+$ ion impact (Figure 8b, orange curve), we observe a rapid decrease in the mass of the C:H film during the first impacts (between 0 and 400 impacts), followed by a much slower decrease. This last phase of mass stabilization could be due to the simultaneous phenomena of sputtering and ion atom incorporation into the surface or the fact that only a very stable C:H film remains, strongly bonded to the surface and lacking active sites for ion incorporation. Taken together, these results show that sputtering of a C:H film with Ar^+ ions (inert) is faster than that with $C_2H_3^+$ ions (reactive).

Furthermore, the behavior of the ions at 50 eV could also explain the negligible influence of these ions on the overall deposition with neutral species (Figure 1b) observed in Section 2.2, their low density still being the main reason.

During the different impacts, we also determined the different carbon clusters that were ejected from the surface (figure not shown here). We identified C_2 clusters (hydrocarbon molecules with two carbon atoms) as the main ejected clusters after the impacts of the different ions (Ar^+ and $C_2H_3^+$), regardless of energy. This large ejection of C_2 clusters compared to other clusters can be attributed to the high-energy impact of the ions, which

causes carbon–carbon bonds to break within the film, resulting in the formation of small, stable clusters.

4 | CONCLUSION

In summary, reactive MD simulations were performed to investigate the mechanisms of hydrocarbon film growth resulting from the interactions of the main neutral species (CH_4 , C_2H_4 , C_2H_2 , C_2H , CH_3 , and H_2) of an Ar/CH_4 plasma on a stainless-steel surface in the temperature range of 300–1000 K. At low temperatures (300–500 K), we observed that the mass of the C:H film was almost constant, and at 1000 K, a decrease in mass of about 10% was observed. The C_2H radical was identified as the main precursor of the C:H film growth at all temperatures, while stable neutral species played an important role in the formation of the first hydrocarbon monolayer (in the first instants of the simulations). On characterizing the C:H films, we found that the C:H films were unsaturated at all temperatures, with a dominance of C=C double bonds and carbon atoms with CN 3 (CN^3). A deposition of all neutral species including the two major ions (Ar^+ and $C_2H_3^+$ with an energy of 50 eV) from the Ar/CH_4 discharge was also performed. The effects of the ions on film growth were negligible due to the small amount of these ions compared to the neutral species. Finally, the C:H film formed at 300 K was separately bombarded with Ar^+ and $C_2H_3^+$ ions at energies of 50, 75, and 100 eV. We observed that at 50 eV, the impact of Ar^+ ions only induced chemical reorganization of the film structure, while for $C_2H_3^+$ ions, we observed incorporation of their atoms into the film, leading to an increase in the mass of the C:H film. At higher energies, we observed more extensive sputtering of the film and also that this sputtering was faster with Ar^+ ions than with $C_2H_3^+$ ions, which can also become incorporated into the film due to their reactive nature.

ACKNOWLEDGMENTS

This work was supported by the National Scholarship Agency of Gabon (ANBG) and the French National Research Agency (ANR) through the MONA project (ANR-18-CE30-0016). We are grateful to the Fédération Calcul Scientifique et Modélisation Orléans Tours (CaSciModOT) for the numerical resources made available to us.

CONFLICT OF INTEREST STATEMENT

The authors declare no conflict of interest.

DATA AVAILABILITY STATEMENT

The data that support the findings of this study are available from the corresponding author upon reasonable request.

ORCID

Pascal Brault  <http://orcid.org/0000-0002-8380-480X>

Armelle Michau  <http://orcid.org/0000-0002-7669-0277>

REFERENCES

- [1] R. Snyders, D. Hegemann, D. Thiry, O. Zabeida, J. Klemberg-Sapieha, L. Martinu, *Plasma Sources Sci. Technol.* **2023**, 32(7), 074001. <https://doi.org/10.1088/1361-6595/acdabc>
- [2] A. H. Lettington, *Carbon* **1998**, 36(5–6), 555. [https://doi.org/10.1016/S0008-6223\(98\)00062-1](https://doi.org/10.1016/S0008-6223(98)00062-1)
- [3] L. Hu, D. S. Hecht, G. Grüner, *Chem. Rev.* **2010**, 110(10), 5790. <https://doi.org/10.1021/cr9002962>
- [4] P. Brault, M. Ji, D. Sciacqua, F. Poncin-Epaillard, J. Berndt, E. Kovacevic, *Plasma Processes Polym.* **2022**, 19(1), 2100103. <https://doi.org/10.1002/ppap.202100103>
- [5] W. Jacob, *Thin Solid Films* **1998**, 326(1–2), 1. [https://doi.org/10.1016/S0040-6090\(98\)00497-0](https://doi.org/10.1016/S0040-6090(98)00497-0)
- [6] M. Zarshenas, K. Moshkunov, B. Czerwinski, T. Leyssens, A. Delcorte, *J. Phys. Chem. C* **2018**, 122(27), 15252. <https://doi.org/10.1021/acs.jpcc.8b01334>
- [7] D. Hegemann, E. Körner, N. Blanchard, M. Drabik, S. Guimond, *Appl. Phys. Lett.* **2012**, 101(21), 211603. <https://doi.org/10.1063/1.4767999>
- [8] A. von Keudell, W. Möller, R. Hytry, *Appl. Phys. Lett.* **1993**, 62(9), 937. <https://doi.org/10.1063/1.108525>
- [9] T. A. Plaisted, S. B. Sinnott, *J. Vac. Sci. Technol. A* **2001**, 19(1), 262. <https://doi.org/10.1116/1.1335683>
- [10] A. von Keudell, W. Jacob, *Prog. Surf. Sci.* **2004**, 76(1–2), 21. <https://doi.org/10.1016/j.progsurf.2004.05.001>
- [11] C. Hopf, K. Letourneur, W. Jacob, T. Schwarz-Selinger, von A. Keudell, *Appl. Phys. Lett.* **1999**, 74(25), 3800. <https://doi.org/10.1063/1.124184>
- [12] P. Pecher, W. Jacob, *Appl. Phys. Lett.* **1998**, 73(1), 31. <https://doi.org/10.1063/1.121713>
- [13] W. Möller, *Appl. Phys. A* **1993**, 56(6), 527. <https://doi.org/10.1007/BF00331402>
- [14] L. E. Kline, W. D. Partlow, W. E. Bies, *J. Appl. Phys.* **1989**, 65(1), 70. <https://doi.org/10.1063/1.343378>
- [15] M. Bauer, T. Schwarz-Selinger, W. Jacob, von A. Keudell, *J. Appl. Phys.* **2005**, 98(7), 073302. <https://doi.org/10.1063/1.2061890>
- [16] G. Otakandza-Kandjani, P. Brault, M. Mikikian, A. Michau, K. Hassouni, *Plasma Processes Polym.* **2023**, 21(2), e2300120. <https://doi.org/10.1002/ppap.202300120>
- [17] G. Tetard, A. Michau, S. Prasanna, J. Mougenot, P. Brault, K. Hassouni, *Plasma Sources Sci. Technol.* **2021**, 30(10), 105015. <https://doi.org/10.1088/1361-6595/ac2a17>
- [18] G. Tetard, A. Michau, S. Prasanna, J. Mougenot, P. Brault, K. Hassouni, *Plasma Processes Polym.* **2022**, 19(5), 2100204. <https://doi.org/10.1002/ppap.202100204>
- [19] G. O. Kandjani, P. Brault, M. Mikikian, G. Tetard, A. Michau, K. Hassouni, *Plasma Processes Polym.* **2023**, 20(4), 2200192. <https://doi.org/10.1002/ppap.202200192>
- [20] C. Deschenaux, A. Affolter, D. Magni, C. Hollenstein, P. Fayet, *J. Phys. D: Appl. Phys.* **1999**, 32(15), 1876. <https://doi.org/10.1088/0022-3727/32/15/316>
- [21] F. Silva, K. Hassouni, X. Bonnin, A. Gicquel, *J. Phys.: Condens. Matter* **2009**, 21(36), 364202. <https://doi.org/10.1088/0953-8984/21/36/364202>
- [22] D. B. Graves, P. Brault, *J. Phys. D: Appl. Phys.* **2009**, 42(19), 194011. <https://doi.org/10.1088/0022-3727/42/19/194011>
- [23] E. C. Neyts, P. Brault, *Plasma Processes Polym.* **2017**, 14(1–2), 1600145. <https://doi.org/10.1002/ppap.201600145>
- [24] D. W. Brenner, O. A. Shenderova, J. A. Harrison, S. J. Stuart, B. Ni, S. B. Sinnott, *J. Phys.: Condens. Matter* **2002**, 14(4), 783. <https://doi.org/10.1088/0953-8984/14/4/312>
- [25] S. J. Stuart, A. B. Tutein, J. A. Harrison, *J. Chem. Phys.* **2000**, 112(14), 6472. <https://doi.org/10.1063/1.481208>
- [26] T. C. O'Connor, J. Andzelm, M. O. Robbins, *J. Chem. Phys.* **2015**, 142(2), 024903. <https://doi.org/10.1063/1.4905549>
- [27] van A. C. T. Duin, S. Dasgupta, F. Lorant, W. A. Goddard, *J. Phys. Chem. A* **2001**, 105(41), 9396. <https://doi.org/10.1021/jp004368u>
- [28] J. Yu, S. B. Sinnott, S. R. Phillpot, *Phys. Rev. B: Condens. Matter Mater. Phys.* **2007**, 75(8), 085311. <https://doi.org/10.1103/PhysRevB.75.085311>
- [29] T.-R. Shan, B. D. Devine, J. M. Hawkins, A. Asthagiri, S. R. Phillpot, S. B. Sinnott, *Phys. Rev. B: Condens. Matter Mater. Phys.* **2010**, 82(23), 235302. <https://doi.org/10.1103/PhysRevB.82.235302>
- [30] L. Schwaedlerlé, P. Brault, C. Rond, A. Gicquel, *Plasma Processes Polym.* **2015**, 12(8), 764. <https://doi.org/10.1002/ppap.201400223>
- [31] J. J. Véghs, D. B. Graves, *Plasma Processes Polym.* **2009**, 6(5), 320. <https://doi.org/10.1002/ppap.200800223>
- [32] E. Neyts, M. Eckert, A. Bogaerts, *Chem. Vap. Deposition* **2007**, 13(6–7), 312. <https://doi.org/10.1002/cvde.200606551>
- [33] W. L. Quan, X. W. Sun, Q. Song, Z. J. Fu, P. Guo, J. H. Tian, J. M. Chen, *Appl. Surf. Sci.* **2012**, 263, 339. <https://doi.org/10.1016/j.apsusc.2012.09.057>
- [34] S. J. Plimpton, A. P. Thompson, *MRS Bull.* **2012**, 37(5), 513. <https://doi.org/10.1557/mrs.2012.96>
- [35] M. S. Daw, S. M. Foiles, M. I. Baskes, *Mater. Sci. Rep.* **1993**, 9(7–8), 251. [https://doi.org/10.1016/0920-2307\(93\)90001-U](https://doi.org/10.1016/0920-2307(93)90001-U)
- [36] X. W. Zhou, H. Wadley, R. A. Johnson, D. J. Larson, N. Tabat, A. Cerezo, A. K. Petford-Long, G. Smith, P. H. Clifton, R. L. Martens, T. F. Kelly, *Acta Mater.* **2001**, 49(19), 4005. [https://doi.org/10.1016/S1359-6454\(01\)00287-7](https://doi.org/10.1016/S1359-6454(01)00287-7)
- [37] X. W. Zhou, R. A. Johnson, H. N. G. Wadley, *Phys. Rev. B: Condens. Matter Mater. Phys.* **2004**, 69(14), 144113. <https://doi.org/10.1103/PhysRevB.69.144113>
- [38] C.-M. Lin, H.-L. Tsai, *Intermetallics* **2011**, 19(3), 288. <https://doi.org/10.1016/j.intermet.2010.10.008>
- [39] D. W. Jacobson, G. B. Thompson, *Comput. Mater. Sci.* **2022**, 205, 111206. <https://doi.org/10.1016/j.commatsci.2022.111206>
- [40] A. P. Thompson, H. M. Aktulga, R. Berger, D. S. Bolintineanu, W. M. Brown, P. S. Crozier, P. J. in 't Veld, A. Kohlmeyer, S. G. Moore, T. D. Nguyen, R. Shan, M. J. Stevens, J. Tranchida, C. Trott, S. J. Plimpton, *Comput. Phys. Commun.* **2022**, 271, 108171. <https://doi.org/10.1016/j.cpc.2021.108171>

- [41] W. Humphrey, A. Dalke, K. Schulten, *J. Mol. Graphics* **1996**, *14*(1), 33. [https://doi.org/10.1016/0263-7855\(96\)00018-5](https://doi.org/10.1016/0263-7855(96)00018-5)
- [42] A. Stukowski, *Modell. Simul. Mater. Sci. Eng.* **2010**, *18*(1), 015012. <https://doi.org/10.1088/0965-0393/18/1/015012>
- [43] T. E. Oliphant, *Comput. Sci. Eng.* **2007**, *9*(3), 10. <https://doi.org/10.1109/MCSE.2007.58>
- [44] I. Géraud-Grenier, M. Mikikian, F. Faubert, V. Massereau-Guilbaud, *J. Appl. Phys.* **2019**, *126*(6), 063301. <https://doi.org/10.1063/1.5099326>
- [45] J. Benedikt, *J. Phys. D: Appl. Phys.* **2010**, *43*(4), 043001. <https://doi.org/10.1088/0022-3727/43/4/043001>
- [46] K. De Bleecker, A. Bogaerts, W. Goedheer, *Phys. Rev. E* **2006**, *73*(2), 026405. <https://doi.org/10.1103/PhysRevE.73.026405>
- [47] A. R. Sharma, R. Schneider, U. Toussaint, K. Nordlund, *J. Nucl. Mater.* **2007**, *363–365*, 1283. <https://doi.org/10.1016/j.jnucmat.2007.01.180>
- [48] D. A. Alman, D. N. Ruzic, *Phys. Scr.* **2004**, *T111*(1), 145. <https://doi.org/10.1238/Physica.Topical.111a00145>
- [49] von A. Keudell, *Thin Solid Films* **2002**, *402*(1–2), 1. [https://doi.org/10.1016/S0040-6090\(01\)01670-4](https://doi.org/10.1016/S0040-6090(01)01670-4)
- [50] J. R. Doyle, *J. Appl. Phys.* **1997**, *82*(10), 4763. <https://doi.org/10.1063/1.366333>
- [51] F. Thiéry, Y. Pauleau, J. J. Grob, D. Babonneau, *Thin Solid Films* **2004**, *466*(1–2), 10. <https://doi.org/10.1016/j.tsf.2004.01.105>
- [52] C. De Bie, B. Verheyde, T. Martens, J. van Dijk, S. Paulussen, A. Bogaerts, *Plasma Processes Polym.* **2011**, *8*(11), 1033. <https://doi.org/10.1002/ppap.201100027>
- [53] W. Bohmeyer, D. Naujoks, A. Markin, I. Arkhipov, B. Koch, D. Schröder, G. Fussmann, *J. Nucl. Mater.* **2005**, *337–339*, 89. <https://doi.org/10.1016/j.jnucmat.2004.10.107>

How to cite this article: G. O. Kandjani, P. Brault, M. Mikikian, A. Michau, K. Hassouni, *Plasma. Process. Polym.* **2024**, e2400084. <https://doi.org/10.1002/ppap.202400084>